

This discussion paper is/has been under review for the journal Atmospheric Chemistry and Physics (ACP). Please refer to the corresponding final paper in ACP if available.

Transport of Saharan dust from the Bodélé Depression to the Amazon Basin: a case study

Y. Ben-Ami¹, I. Koren¹, Y. Rudich¹, P. Artaxo², S. T. Martin³, and M. O. Andreae⁴

¹Department of Environmental Sciences and Energy Research, Weizmann Institute of Science, Rehovot, Israel

²Institute of Physics, University of São Paulo, São Paulo, Brazil

³School of Engineering and Applied Sciences and Department of Earth and Planetary Sciences, Harvard University, Cambridge, Massachusetts, USA

⁴Biogeochemistry Department, Max Planck Institute for Chemistry, Mainz, Germany

Received: 26 January 2010 – Accepted: 28 January 2010 – Published: 12 February 2010

Correspondence to: Y. Ben-Ami (yuval.ben-ami@weizmann.ac.il)

Published by Copernicus Publications on behalf of the European Geosciences Union.

4345

Abstract

Through long-range transport of dust, the Sahara desert supplies essential minerals to the Amazon rain forest. Since Saharan dust reaches South America mostly during the Northern Hemisphere winter, the dust sources active during winter are the main contributors to the forest. Given that the Bodélé depression area in Southwestern Chad is the main winter dust source, a close link is expected between the Bodélé emission patterns and volumes and the mineral supply flux to the Amazon.

Until now, the particular link between the Bodélé and the Amazon forest was based on sparse satellite measurements and modeling studies. In this study, we combine a detailed analysis of space-borne and ground data with reanalysis model data and surface measurements taken in the Central Amazon during the Amazonian Aerosol Characterization Experiment (AMAZE-08) in order to explore the validity and the nature of the proposed link between the Bodélé depression and the Amazon forest.

This case study follows the dust events of 11–16 and 18–27 February 2008, from the emission in the Bodélé over West Africa, the crossing of the Atlantic Ocean, to the observed effects above the Amazon canopy about 10 days after the emission. The dust was lifted by surface winds stronger than 14 m s^{-1} , usually starting early in the morning. The lofted dust mixed with biomass burning aerosols over Nigeria, was transported over the Atlantic Ocean, and arrived over the South American continent. The top of the aerosol layer reached above 3 km, and the bottom merged with the marine boundary layer. The arrival of the dusty air parcel over the Amazon forest increased the average concentration of aerosol crustal elements by an order of magnitude.

1 Introduction

Mineral dust has been suggested to play an important role in biogeochemical cycles (Jickells et al., 2005; Mahowald et al., 2009; Falkowski et al., 1998; Garrison, et al., 2003), climatic processes (Ramanathan et al., 2001; Rosenfeld et al., 2001; Stith et al.,

4346

2009; Levin et al., 1996; Teller and Levin, 2006; Albrecht, 1989; Jiang et al., 2006; Kaufman et al., 2005c; Koren et al., 2005; Twomey, 1974; Falkowski et al., 1998), and human life (Prospero, 1999; Griffin and Kellogg, 2004).

5 Despite major efforts, the spatial and temporal distributions of mineral dust remain uncertain. Therefore, the nature and magnitude of dust feedbacks on climatic processes, biogeochemical cycles, and human life are not well constrained. Important unanswered questions include: what are the exact Saharan dust sources of crustal elements observed in the Amazon Basin and what are their associated fluxes?

10 The Amazon rain forest has important roles in Earth's climate system. It acts as a source of primary and secondary biogenic aerosol particles and components (Artaxo and Hansson, 1994; Martin et al., 2009a; Quéré et al., 2009). It also affects the global biogeochemical cycles, including carbon cycling (Davidson and Artaxo, 2004). To sustain the well-being of the forest and the fragile balance between the rain forest and the atmosphere, the Amazon forest must receive a sufficient amount of nutrients. 15 However, the intense precipitation and ensuing floods wash most of the soluble nutrients from the rainforest soil, leaving behind a quite infertile soil, with limited mineral nutrients available for plant growth (Vitousek and Sanford, 1986).

In-situ measurements (Talbot et al., 1990) and image analysis studies (Swap et al., 1992) have suggested that the deficiency of minerals in the Amazon soil can be replenished by deposition of mineral dust, mostly from the Sahara. Indeed, elements found in dust such as Al, Ti and Fe were previously observed in the Amazon region (e.g., Artaxo et al., 1990; Formenti et al., 2001). However, the exact origin of the dust settling in the Amazon, as well as the magnitude and the frequency of the transported quantities are not well known. An important reason for these uncertainties is that previous studies 25 (e.g., Swap et al., 1992; Formenti et al., 2001; Ansmann et al., 2009) were restricted either to the Saharan region or to the Amazon forest, and so the direct link of the dust's transport route could not be studied in sufficient detail.

Koren et al. (2006) have suggested that the Bodélé depression, which is located in Chad (centered near 17° N 18° E), is the main source for the dust transported to the

4347

Amazon Basin. Using a year-long satellite data set, they studied the emission pattern of the Bodélé, and suggested a dust transport route towards the Amazon. However, their study did not include ground-based measurements, and their conclusions were based on inductive reasoning, showing that the Saharan dust arrives in the Amazon mostly 5 during the (Northern Hemisphere) wintertime and that the Bodélé is the main winter source. Therefore, they concluded that the Bodélé contributes a significant amount of nutrients to the Amazon Basin.

Other regional (e.g., Schepanski et al., 2007; Ginoux et al., 2009) and global (e.g., Prospero et al., 2002) remote sensing studies also identified the Bodélé depression 10 as one of the most active dust sources. The Bodélé depression is characterized by a year-long activity and a dust emission peak during the Northern Hemisphere winter months, with estimated emissions of $(58 \pm 8) \times 10^6$ tonnes (estimated for winter-spring of 2003–2004), equivalent to emissions of more than 7×10^5 tonnes per emission day (Koren et al., 2006). The uniqueness of the Bodélé as a prime dust source was attributed to three factors: A. Mineralogy – being part of the former lake Mega-Chad, 15 the Bodélé ($\sim 133\,532 \text{ km}^2$) is a rich dust reservoir, including low density diatomite and eroded diatomite sand (Bristow et al., 2009), composed of SiO_2 and small quantities of Al_2O_3 and Fe (Chappell et al., 2008); B. Meteorology – The Harmattan winds from the Low Level Jet (Washington and Todd, 2005) and, C. Topography – the persistent surface winds blowing southwestward are focused toward the Bodélé depression by the structure of the valley between the Tibesti ($\sim 2600 \text{ m}$) and Ennedi ($\sim 1000 \text{ m}$) massifs (Koren et al., 2006).

20 During the winter months, dust emitted from the Bodélé depression is transported by the Harmattan winds southwestward over the Sahel toward the Gulf of Guinea into the Atlantic Ocean heading to the coast of South America (Kaufman et al., 2005a). This transport route arises from the shift to the south of the Inter Tropical Convergence Zone.

The extensive emitted dust mass, the tropical Atlantic northwesterly winds regime, and the observed crustal elements found in dust in the Amazon Basin suggest that

4348

Saharan dust reaches the Amazon forest. The exact Saharan dust sources, and the amount of Saharan dust that actually reaches the Amazon forest, however, remains challenging. Herein, we present a detailed case study that integrates the data analysis approach to track Bodélé's dust to the Amazon region.

5 2 Methods

The objectives of AMAZE-08 were to understand the sources and processes that regulate emissions, transformation and deposition of biogenic aerosol particles in the forest. Extensive ground based measurements were conducted between 7 February and 14 March 2008 during the wet season. The AMAZE-08 site was 60 km NNW of Manaus and located within a mostly pristine rainforest (Martin et al., 2009b, 2010).

We analyzed Saharan dust emissions and transport along the dust route during this period, using surface and remote sensing measurements. The surface wind speed and azimuth were estimated by probing the propagation of a dust front between the morning overpass of the MODerate resolution Imaging Spectroradiometer (MODIS) instrument on board Terra and the afternoon MODIS-Aqua satellites measurements, using the 1 km resolution blue band (440 nm) data (Koren and Kaufman, 2004). Time of emission in Africa was estimated by back propagating the dust front to the source, using the derived wind speed. Dust passage was monitored at the Ilorin AEROSOL RObotic NETWORK (AERONET, Holben et al., 1998) station located in Nigeria (8°19' 12 N, 4°20' 24 E), along the dust pathway. Back trajectories of the dust-containing air parcels were calculated based on the National Center for Environmental Prediction (NCEP) analysis (Kalnaya et al., 1996).

Dust mass was estimated at two locations, close to the source and over the ocean:

A. Near dust sources, which are far from any others aerosol sources, the observed Aerosol Optical Depth (AOD) was attributed solely to dust. The dust AOD was transformed to dust mass, M_{du} , using the following relation:

$$M_{du} = 2.7A\tau_{du}(g) \quad (1)$$

4349

where A is the plume area (in 1 km resolution) and τ_{du} is the mean dust AOD at the 550 nm band (at 10 km resolution) of the MODIS instrument (based on the deep blue data; Hsu et al., 2006) located on Aqua. The factor $2.7 (\pm 0.4) \text{ gm}^{-2}$ is a result of regression calculations between the AOD in the visible (550 nm) and aerosol column concentration, based on several in-situ measurements in the Sahara region (see Kaufmann et al., 2005a and the related references listed therein; Yu et al., 2009).

B. Over the Atlantic Ocean, it is likely that dust particles are mixed with marine aerosol (sea salt, organic matter and oxidation products of dimethyl sulfide; Yu et al., 2009) and biomass-burning aerosols from the Sahel region (Andreae et al., 1986; Formenti et al., 2008; Ansmann et al., 2009). This mixing increases the fine fraction, f , defined as the aerosol fraction with diameter smaller than $1 \mu\text{m}$ (Kaufmann et al., 2005b). Therefore, over the ocean, the daily dust mass, M_{du} , was estimated from Eq. (1), where A is the area over the ocean covered by dust (between 25° N–15° S, and 50° W–15° E). τ_{du} was extracted from the total AOD, τ , and from f , using Eq. (2) (Kaufmann et al. 2005a; Yu et al., 2009):

$$\tau_{du} = \frac{\tau(f_a - f) - \tau_m(f_a - f_m)}{f_a - f_d} \quad (2)$$

τ and f were products of the 550 nm band of the MODIS instrument (both in 1° resolution) located on the Terra and Aqua satellites. f_a , f_m , and f_d are the anthropogenic, maritime and dust fine fractions (0.90, 0.45 and 0.37, respectively, with estimated error of 20%) as estimated over selected regions (Yu et al., 2009). The AOD attributed to maritime aerosol, τ_{ma} , was based on Eq. (3) (Smirnov et al., 2003; Kaufmann et al., 2005a):

$$\tau_{ma} = 0.007W \pm 0.02 \quad (3)$$

where W is the magnitude of the wind speed at 1000 hPa, obtained from the NCEP reanalysis.

The propagation of the dust/biomass-burning plumes was further analyzed by studying the polarization signal of the plumes, using the Cloud-Aerosol Lidar with Orthogonal

Polarization (CALIOP) instrument on board the Cloud-Aerosol Lidar and Infrared Pathfinder Satellite Observation (CALIPSO) satellite (Thomason et al., 2007). In order to enhance the backscatter signal, the vertical (up to 8 km) and the horizontal resolution of the profiles were reduced to 60 m (2 signal points) and 5 km (15 signal points), respectively. In contrast to other types of aerosols, dust plumes are dominated by nonspherical particles, and therefore their depolarization signal (i.e., the ratio of the perpendicular to parallel components of the 532 nm band, including aerosol and molecular scattering) is expected to be relatively high (Murayama et al., 2001), approximately between 0.1 to 0.4 (Liu et al., 2008, 2008a, b).

The distinction between aerosols and clouds was based on (a) the depolarization signal and (b) the different backscatter patterns (Ben Ami et al., 2009): we assumed that clouds have strong backscatter signal, and either (a) sporadic and large vertical dimension (cumulus clouds) or (b) continuous horizontal shape (stratiform clouds). Aerosol plumes, on the other hand, have a continuous horizontal and vertical structure with wide horizontal dimension and weaker backscatter signal.

The propagation of the dust over the Atlantic Ocean was also studied by analyzing the spatial distribution of the AOD from MODIS along the center of the dust/biomass-burning plumes (between 10° N–5° S, and 50° W–10° E).

At the AMAZE-08 field station (2°35'22" S, 60°06'55" W), aerosol particles having diameters smaller than 2.0 µm as well as those in the size range from 2.0 to 10 µm were collected from above the rain forest canopy, using Stacked Filter Units with Nuclepore filters. Elemental analysis of collected particles was carried out by Particle Induced X-ray Emission (PIXE) (Artaxo et al., 1987).

3 Results

The results are presented in four stages, from source to sink, showing correlations that link each subsequent stage to the previous one:

1. Analysis of the Bodélé depression emission pattern.

4351

2. Back trajectories and analysis of aerosol properties over the Ilorin AERONET station near the Gulf of Guinea.

3. Analysis of the transport of air masses over Africa and over the Atlantic Ocean

4. Elemental analysis (by PIXE) of aerosols collected at the AMAZE-08 field site in Central Amazonia.

3.1 Analysis of the Bodélé depression emission pattern

During February 2008, the activity in the Bodélé depression (Fig. 1) was characterized by two periods of dust emission between 6–8 and 11–16 February, followed by an extensive emission between 18–27 February. During early and mid-March, the Bodélé was significantly less active. On a few occasions, the activity in the Bodélé was accompanied by significant emissions from other sources along the Moroccan coastline. These plumes, for the most part, propagated northwest, away from the South American coastline. Additional dust activity with much smaller magnitude was observed in other nearby sources.

Frequently, the dust originated from the Bodélé is emitted from two sources: the main source area, northeast and within the large ephemeral lake (point 1 in Fig. 1b and c) and a second smaller source area 150 km south of the lake which is not always active (point 2 in Fig. 1b and c).

The emission pattern analysis is based on five emission days (16, 20, 24, 25 February and 22 March) that were selected based on MODIS coverage during the study period. The emission started during the early morning hours, approximately between 03:30 LT to 06:30 LT, with surface wind speeds between 14.5 to 18 m s⁻¹ and wind azimuth between 225° and 250°. The emitted plumes, observed by the Aqua satellite, covered an area between 12×10³ and 100×10³ km². The average AOD of the plumes varied between 2 and 3.9, and the emitted mass per emission day (up to about 12:30 LT) varied between 1×10⁵ and 1×10⁶ tonnes. The emitted mass was equivalent to an emission flux between 2.8 and 166.8 tonnes s⁻¹.

4352

The estimated time of emission, surface wind azimuth and emission flux are in agreement with the analysis of Koren and Kaufman (2004) and Koren et al. (2006). The estimated surface wind speed is slightly higher than measurements done by Koren and Kaufman (2004) and Koren et al. (2006); however, it is in line with the suggested minimum threshold speed for dust emission of $10\text{--}11\text{ m s}^{-1}$ (Koren and Kaufman, 2004; Todd et al., 2007).

A special case is the dust emission during 18 February, which was characterized by early emission (starting approximately at 23:30) and a large emitted mass of $\sim 2 \times 10^6$ tonnes (up to noon local time). The extensive dust emission continued on 19 February. The emission of the Bodélé then persisted for seven more days until 27 February.

3.2 Back trajectories and analysis of aerosol properties over Ilorin

Focusing on two emission periods, 11–16 and 18–27 February, we followed the dust plumes along their routes westward toward the Gulf of Guinea. During 14–16 and 20–22 February, the Ilorin AERONET station (located at $8^\circ 19' \text{ N}$, $4^\circ 20' \text{ E}$) measured a significantly increased AOD accompanied by a decrease of the Angstrom exponent (\AA , Eck et al., 1999). Small \AA values indicate the presence of large particles such as dust. Significant emissions, starting on 18 February, are reflected in the AOD values (Fig. 2a). Back trajectory calculations from Ilorin station, during 14–16 and 20–22 February, suggest that the air masses passed over the Bodélé region (Fig. 2b) and that the transport time was ~ 2.5 days.

3.3 Analysis of the transport of air masses over Africa and over the Atlantic Ocean

The propagation of the dust plumes over North Africa was analyzed using CALIOP vertical profiles. Over the Atlantic Ocean, we used CALIOP and MODIS measurements. Figure 3a and b shows the propagation of the dust plume during the study

4353

period, beginning near the source, continuing over the Atlantic and finally toward the Amazon Basin. It can be seen that the dust event is composed of two major plumes (as observed by MODIS, Fig. 1c) with top heights near 1.2 and 2 km (for 19 February), both emitted from the Bodélé. As the dust propagated southwest from the Bodélé, it mixed with biomass burning smoke (Fig. 3a,b). From the mixing region over Nigeria, the dust and the biomass smoke continued together, as shown in the depolarization analysis. The comparison between Fig. 3a and b with observations from a day without a dense aerosol plume (Fig. 4) clearly emphasizes the presence of the dust and the biomass-burning aerosols over the marine boundary layer during the period of the study.

3.3.1 Depolarization analysis

The histogram of the depolarization signal of the aerosol plume, retrieved from the vertical profiles of CALIOP, showed that most of the values fell between ~ 0.1 to ~ 0.4 (Fig. 5). These depolarization values, which are typical for dust (Liu et al., 2008, 2008a, b), indicate that the majority of the observed signal (during the period of the study) was obtained from dust particles. Water clouds located near or within the aerosol plume, have higher depolarization values (between 0.4 to 1) due to multiple scattering and were a minor contribution to the overall sampled signal. Anthropogenic aerosols, such as biomass smoke, and molecules, which are much smaller compared to the CALIOP wavelength, have low (between 0 to 0.1) depolarization values (Liu et al., 2008, 2008a, b).

Most of the signal is attributed to dust since most of the depolarization data is within 0.1–0.4. To emphasize the location of cleaner dust within the transported aerosol plume, we showed (Fig. 6a) regions where the depolarization signal is larger than 0.25 (the threshold is marked on Fig. 5) and smaller than 0.4. This relatively high value indicates that the selected regions are dominated by dust.

Based on this assumption, several regions of relatively pure dust, as well as regions characterized by biomass burning mixed with dust (with lower depolarization values),

4354

are marked in Fig. 6a. Close to the source (19 February), the aerosol plume is composed of (a) biomass burning mixed with dust in the southern parts of the aerosol plume (depolarization signal of 0.19), (b) relatively pure dust in the central part of the plume (depolarization signal of 0.31) and (c) pollution (depolarization between 0 to ~0.13), most likely transported from Europe via the Mediterranean Sea (Duncan et al., 2008), in the northern part (Fig. 6a). The tri-modal distribution of these aerosols is also evident in Fig. 6b. The depolarization values of ~0.3 are in line with previous studies, and the depolarization value of ~0.19 is significantly larger than that of <0.1 expected for pure biomass smoke (Liu et al., 2008, 2008a, b), indicating that the biomass smoke is mixed with dust particles.

The mixing of both types of aerosol over the Atlantic Ocean, as well as sedimentation of large dust particles along the transport route, is also evident from the shift of the center of the depolarization distribution (Fig. 6b) from 0.32 over Africa to 0.15 over the Western Atlantic.

Detailed analysis of the regions that are dominated by dust (marked with red in Fig. 6a) shows that the depolarization signal decreases over time during transport, possibly due to extensive sedimentation of large dust particles. An opposite trend of increasing depolarization signal (from 0.19 to 0.22) characterized the regions that are dominated by biomass burning mixed with dust (marked with green on Fig. 6a), indicating that more dust is dissipating toward the air mass containing the biomass burning. Further west (22–24 February), the depolarization decreases again, most likely due to aerosol wet removal and sedimentation.

3.3.2 Analysis with MODIS AOD

As the dust plume continued to move away from its source, the spectral signal of the dust weakened, and it was more difficult to observe the dust via MODIS's spectral bands. However, the spatial and temporal distribution of MODIS AOD, calculated as latitudinal daily averages along the center of the plume, clearly shows a significant increase of AOD, approximately from 17 February to 1 March (Fig. 7a). The spatial

4355

and temporal distribution of the fine fraction (f), also calculated as latitudinal daily averages along the center of the plume (not shown), is in good agreement with the spatial and temporal pattern of the AOD. The suggestion is that periods of high AOD were characterized by the presence of a significant coarse fraction, presumably dust. The longitudinal distribution of the AOD, which extended from the African coast to the South American coast (50° W), suggests the arrival of Saharan dust as far as the edge of the Amazon region. Estimation of dust loading (Fig. 7b) shows that the extensive dust emission increased the dust loading over the ocean (between 20° N–15° S, and 50° W–15° E) by more than 100%. The spatial distribution of the AOD from 17 February to 1 March is composed of minor and major peaks (marked in Fig. 7a) that are simultaneous with the two events of dust emissions that occurred during 11–16 and 18–27 February, including the signature of these emissions in the Ilorin AERONET measurements (14–16 and 20–22 February). The upper part of Fig. 7a,b (~5–9 February and ~14–15 March) show evidence for two other emissions periods.

3.4 Elemental analysis (by PIXE) of aerosols collected at the AMAZE-08 field site in Central Amazonia

The arrival of the dust in the Amazon region was observed at the AMAZE-08 field site between 22 and 26 February. Elemental analysis by PIXE of the aerosol showed an increase in the elements Si, Al, Fe, Mn and Ti in the coarse and the fine fraction, all attributed to mineral dust emitted during 18–27 February (and possibly even earlier, during 11–16 February) from the Bodélé depression (Fig. 8). The significant increase in the observed crustal elements continued until about 4 March. During this period, the daily averaged concentration of the previously mentioned crustal elements increased by approximately one order of magnitude (i.e., from 0.076 to 0.79 $\mu\text{g m}^{-3}$ and from 0.062 to 0.82 $\mu\text{g m}^{-3}$ in the fine and coarse modes, respectively). The total mass of the above crustal elements during this period (between 22 February and 4 March) was 4.83 $\mu\text{g m}^{-3}$. Increases in other elements (not shown), such as S (in the coarse fraction), also occurred, most likely contributed by marine sources, possibly

4356

originating from dimethyl sulfide (DMS) oxidation. Chloride also in the coarse fraction indicated that the dusty air plume passed over the ocean and mixed with sea salt, as expected. Potassium, in the fine and coarse fraction, may be attributed to a contribution of biomass burning aerosol, possibly originating from the Southern Sahel region. 5 The increase in crustal elements during additional periods, as seen in Fig. 8 (e.g.: during 5–9 April), suggests that this is not a singular event and that there are additional cases of Saharan dust transport to the Amazon Basin. Analysis of CALIOP profiles along the Brazilian coastline (for 24 February, Fig. 3a) showed that the aerosol plume attained a maximum height near 3.3 km, while its base merged with the underlying 10 marine boundary layer.

4 Conclusions

Koren et al. (2006) suggested the Bodélé as source of nutrients for the Amazon Basin based on inductive reasoning without showing evidence for dust deposition. Here we present a detailed case study that closely follows dust emitted from the Bodélé depression in Chad and deposited in the Amazon Basin. The AMAZE-08 measurements in the 15 Central Amazon show episodes of dust, biomass burning and marine aerosol elements, in agreement with the expected arrival time of the dust-laden air from the Bodélé, as retrieved by remote sensing measurements. The arrival of dust in the Amazon Basin is also in line with simultaneous in situ measurements from AMAZE-08, showing enhancement in ice nuclei due to the presence of the dust particles (Prenni et al., 2009). 20 The travel time from the source region to the Amazon Basin is approximately 10 days.

Nonetheless, despite the dominance of the Bodélé dust emissions, it is fair to assume contributions from additional dust sources along the transport path. We also assume that not all dust episodes (during winter in the Northern Hemisphere) reach 25 the Amazon forest. For example, Lidar observations (Ansmann et al., 2009) from one month before our case study (15 January to 14 February 2008), showed that dust/biomass-burning plumes that originated from the Sahara and were transported

4357

westward, were almost depleted of dust particles when they reached the Amazon region.

The Bodélé emission rates might be underestimated due to saturation of the AOD inversion algorithm (at \sim AOD=4) and the use of an AOD-to-mass conversion constant 5 that is based on a compilation of many in situ dust measurements (Kaufman et al., 2005a; Yu et al., 2009) and therefore should reflect average dust events and underestimate strong dust events. Moreover, our data is limited to the last daily satellite snapshots taken around 13:30 LT and therefore do not include dust that was emitted 10 during the local afternoon (after the pass of the Aqua satellite over the region). Based on the spatial and temporal distribution of the depolarization signal and the estimation of dust loading, we show that the Bodélé's activity is clearly reflected by changes in aerosol size distribution and dust loading over the tropical Atlantic. Although further studies are needed, our study suggests that in addition, events with early emission starting time (around midnight) are likely to be strong dust events and are more likely 15 to be transported and to reach the Amazon forest (during the winter season).

Acknowledgements. This research was partly funded by the Minerva foundation, with funding from the Federal German Ministry for Education and Research, and the German Israeli Science Foundation (GIF) Contract no. I-899-228.10/2005. Y. R. acknowledges support by the Helen and Martin Kimmel Award for Innovative Investigation. B.-A. Y. acknowledges Mr. Jeremy 20 Seltzer for proofreading.

References

- Albrecht, B. A.: Aerosols, cloud microphysics, and fractional cloudiness, *Science*, 245, 1227–1230, 1989.
- Andreae, M. O., Charlson, R. J., Bruynseels, F., Storms, H., and Grieken, R. V.: Internal mixture of sea salt, silicates, and excess sulfate in marine aerosols, *Science*, 232, 1620–1623, 1986. 25
- Ansmann, A., Baars, H., Tesche, M., Müller, D., Althausen, D., Engelmann, R., Pauliquevis, T., and Artaxo, P.: Dust and smoke transport from Africa to South America: lidar

4358

- profiling over Cape Verde and the Amazon rainforest, *Geophys. Res. Lett.*, 36, L11802, doi:10.1029/2009GL037923, 2009.
- Artaxo, P. and Orsini, C.: PIXE and receptor models applied to remote aerosol source apportionment in Brazil, *Nucl. Instrum. Methods*, B22, 259–263, 1987.
- 5 Artaxo, P., Maenhaut, W., Storms, H., and Grieken, R. V.: Aerosol characteristics and sources for the Amazon Basin during the wet season, *J. Geophys. Res.*, 95, 16971–16986, 1990.
- Artaxo, P. and Hansson, H. C.: Size distribution of biogenic aerosol particles from the Amazon Basin, *Atmos. Environ.*, 29, 393–402, 1994.
- Ben-Ami, Y., Koren, I., and Altaratz, O.: Patterns of North African dust transport over the Atlantic: winter vs. summer, based on CALIPSO first year data, *Atmos. Chem. Phys.*, 9, 7867–7875, 2009, <http://www.atmos-chem-phys.net/9/7867/2009/>.
- 10 Bristow, C., Drake, N., and Armitage, S.: Deflation in the dustiest place on Earth: the Bodélé Depression, Chad, *Geomorphology*, 105, 50–58, 2009.
- 15 Chappell, A., Warren, A., O'Donoghue, A., Robinson, A., Thomas, A., and Bristow, C.: The implications for dust emission modeling of spatial and vertical variations in horizontal dust flux and particle size in the Bode'le Depression, Northern Chad, *J. Geophys. Res.*, 113, D04214, doi:10.1029/2007JD009032, 2008.
- Davidson, E. A. and Artaxo, P.: Globally significant changes in biological processes of the Amazon Basin: results of the Large-Scale Biosphere-Atmosphere Experiment, *Global Change Biol.*, 10, 1–11, 2004.
- Duncan, B. N., West, J. J., Yoshida, Y., Fiore, A. M., and Ziemke, J. R.: The influence of European pollution on ozone in the Near East and northern Africa, *Atmos. Chem. Phys.*, 8, 2267–2283, 2008, <http://www.atmos-chem-phys.net/8/2267/2008/>.
- 25 Eck, T. F., Holben, B. N., Reid, J. S., Dubovik, O., Smirnov, A., O'Neill, N. T., Slutsker, I., and Kinne, S.: Wavelength dependence of the optical depth of biomass burning, urban, and desert dust aerosols, *J. Geophys. Res.*, 104, 31333–31349, 1999.
- Falkowski, P. G., Barber, R. T., and Smetacek, V.: Biogeochemical controls and feedbacks on ocean primary production, *Science*, 281, 200–206, 1998.
- 30 Formenti, P., Andreae, M. O., Lange, L., Roberts, G., Cafmeyer, J., Rajta, I., Maenhaut, W., Holben, B. N., Artaxo, P., and Lelieveld, J.: Saharan dust in Brazil and Suriname during the Large-Scale Biosphere-Atmosphere Experiment in Amazonia (LBA) – Cooperative LBA

4359

- Regional Experiment (CLAIRE) in March 1998, *J. Geophys. Res.*, 106, 14919–14934, 2001.
- Formenti, P., Rajot, J. L., Desboeufs, K., Caquineau, S., Chevaillier, S., Nava, S., Gaudichet, A., Journet, E., Triquète, S., Alfaro, S., Chiari, M., Haywood, J., Coe, H., and Highwood, E.: Regional variability of the composition of mineral dust from Western Africa: results from the AMMA SOP0/DABEX and DODO field campaigns, *J. Geophys. Res.*, 113, D00C13, doi:10.1029/2008JD009903, 2008.
- 5 Garrison, V. H., Shinn, E. A., Foreman, W. T., Griffin, D. W., Holmes, C. M., Kellogg, C. A., Majewski, M. S., Richardson, L. L., Ritchie, K. B., and Smith, G. W.: African and Asian dust: from desert soils to coral reefs, *Bioscience*, 53, 469–480, 2003.
- 10 Ginoux, P., Garbuzov, D., and Hsu, N. C.: Identification of anthropogenic and natural dust sources using Moderate Resolution Imaging Spectroradiometer (MODIS) Deep Blue Level 2 data, *J. Geophys. Res.*, doi:10.1029/10.2009JD012398, in press, 2009.
- Griffin, D. W. and Kellogg, C. A.: Dust storms and their impact on ocean and human health: dust in earth's atmosphere, *Ecohealth*, 1, 248–295, 2004.
- 15 Gunthe, S. S., King, S. M., Rose, D., Chen, Q., Roldin, P., Farmer, D. K., Jimenez, J. L., Artaxo, P., Andreae, M. O., Martin, S. T., and Pschl, U.: Cloud condensation nuclei in pristine tropical rainforest air of Amazonia: size-resolved measurements and modeling of atmospheric aerosol composition and CCN activity, *Atmos. Chem. Phys.*, 9, 7551–7575, 2009, <http://www.atmos-chem-phys.net/9/7551/2009/>.
- 20 Holben, B. N., Eck, T. F., Slutsker, I., Tanre, D., Buis, J. P., Setzer, A., Vermote, E., Reagan, J. A., Kaufman, Y. J., Nakajima, T., Lavenu, F., Jankowiak, I., and Smirnov, A.: AERONET – a federated instrument network and data archive for aerosol characterization, *Remote Sens. Environ.*, 66(1), 1–16, 1998.
- Hsu, N. C., Tsay, S. C., King, M. D., and Herman, J. R.: Aerosol properties over bright-reflecting source regions, *IEEE T. Geosci. Remote*, 42, 557–569, 2004.
- 25 Jiang, H., Xue, H., Teller, A., Feingold, G., and Levin, Z.: Aerosol effects on the lifetime of shallow cumulus, *Geophys. Res. Lett.*, 33, L14806, doi:10.1029/2006GL026024, 2006.
- Jickells, T. D., An, Z. S., Andersen, K. K., Baker, A. R., Bergametti, G., Brooks, N., Cao, J. J., Boyd, P. W., Duce, R. A., Hunter, K. A., Kawahata, H., Kubilay, N., laRoche, J., Liss, P. S., Mahowald, N., Prospero, J. M., Ridgwell, A. J., Tegen, I., and Torres, R.: Global iron connections between desert dust, ocean biogeochemistry and climate, *Science*, 308, 67–71, 2005.
- 30

4360

- Kalnay, E., Kanamitsu, M., Kistler, R., Collins, W., Deaven, D., Gandin, L., Iredell, M., Saha, S., White, G., Woollen, J., Zhu, Y., Leetmaa, A., Reynolds, R., Chelliah, M., Ebisuzaki, W., Higgins, W., Janowiak, J., Mo, K. C., Ropelewski, C., Wang, J., Jenne, R., and Joseph, D.: The NCEP/NCAR 40-year reanalysis project, *B. Am. Meteorol. Soc.*, *77*, 437–471, 1996.
- 5 Kaufman, Y. J., Koren, I., Remer, L. A., Tanre, D., Ginoux, P., and Fan, S.: Dust transport and deposition observed from the Terra-Moderate Resolution Imaging Spectroradiometer (MODIS) spacecraft over the Atlantic Ocean, *J. Geophys. Res.*, *110*, D10S12, doi:10.1029/2003JD004436, 2005a.
- Kaufman, Y. J., Boucher, O., Tanre, D., Chin, M., Remer, L., and Takemura, T.: Aerosol anthropogenic component estimated from satellite data, *Geophys. Res. Lett.*, *32*, L17804, doi:10.1029/2005GL023125, 2005b.
- Kaufman, Y. J., Koren, I., Remer, L. A., Rosenfeld, D., and Rudich, Y.: The effect of smoke, dust and pollution aerosol on shallow cloud development over the Atlantic Ocean, *P. Natl. Acad. Sci. USA*, *102*(32), 11207–11212, 2005c.
- 15 Koren, I. and Kaufman, Y. J.: Direct wind measurements of Saharan dust events from Terra and Aqua satellites, *Geophys. Res. Lett.*, *31*, L06122, doi:10.1029/2003GL019338, 2004.
- Koren, I., Kaufman, Y. J., Rosenfeld, D., Remer, L. A., and Rudich, Y.: Aerosol invigoration and restructuring of Atlantic convective clouds, *Geophys. Res. Lett.*, *32*, L14828, doi:10.1029/2005GL023187, 2005.
- 20 Koren, I., Kaufman, Y. J., Washington, R., Todd, C. C., Rudich, Y., Martins, J. V., and Rosenfeld, D.: The Bodélé Depression: a single spot in the Sahara that provides most of the mineral dust to the Amazon forest, *Environ. Res. Lett.*, *1*, 1–5, 2006.
- Levin, Z., Ganor, E., and Gladstein, V.: The effects of desert particles coated with sulfate on rain formation in the Eastern Mediterranean, *J. Appl. Meteorol.*, *35*, 1511–1523, 1996.
- 25 Liu, D., Wang, Z., Liu, Z., Winker, D., and Trepte, C.: A height resolved global view of dust aerosols from the first year CALIPSO lidar measurements, *J. Geophys. Res.*, *113*, D16214, doi:10.1029/2007JD009776, 2008a.
- Liu, Z., Omar, A., Vaughan, M., Hair, J., and Kittaka, C.: CALIPSO lidar observations of the optical properties of saharan dust: a case study of long-range transport, *J. Geophys. Res.-Atmos.*, *113*, D07207, doi:10.1029/2007JD008878, 2008b.
- 30 Liu, Z., Liu, D., Huang, J., Vaughan, M., Uno, I., Sugimoto, N., Kittaka, C., Trepte, C., Wang, Z., Hostetler, C., and Winker, D.: Airborne dust distributions over the Tibetan Plateau and surrounding areas derived from the first year of CALIPSO lidar observations, *Atmos. Chem.*

4361

Phys., *8*, 5045–5060, 2008,

<http://www.atmos-chem-phys.net/8/5045/2008/>.

- Mahowald, N., Engelstaedter, S., Luo, C., Sealy, A., Artaxo, P., Benitez-Nelson, C., Bonnet, S., Chen, Y., Chuang, P. Y., Cohen, D. D., Dulac, F., Herut, B., Johansen, A. M., Kubilay, N., Losno, R., Maenhaut, W., Paytan, A., Prospero, J. M., Shank, L. M., and Siefert, R. L.: Atmospheric Iron deposition: global distribution, variability and human perturbations, *Ann. Rev. Marine Sci.*, *1*, 245–278, doi:10.1146/annurev.marine.010908.163727, 2009.
- 5 Martin, S. T., Andreae, M. O., Artaxo, P., Baumgardner, D., Chen, Q., Goldstein, A. H., Guenther, A., Heald, C. L., Mayol-Bracero, O. L., McMurry, P. H., Pauliquevis, T., Pöschl, U., Prather, K. A., Roberts, G. C., Saleska, S. R., Silva Dias, M. A., Spracklen, D. V., Swietlicki, E., and Trebs, I.: Sources and properties of Amazonian aerosol particles, *Rev. Geophys.*, doi:10.1029/2008RG000280, in press, 2009a.
- Martin, S. T., Artaxo, P., Andreae, M. O. et al.: Amazonian Aerosol Characterization Experiment 2008 (AMAZE-08), *Atmos. Chem. Phys.*, in preparation, 2009b.
- 15 Murayama, T., Sugimoto, N., Uno, I., Kinoshita, K., Aoki, K., Hagiwara, N., Liu, Z., Matsui, I., Sakai, T., Shibata, T., Arao, K., Sohn, B.-J., Won, J.-G., Yoon, S.-C., Liy, T., Zhou, J., Hu, H., Aboy, M., Iokibe, K., Koga, R., and Iwasaka, Y.: Ground-based network observation of Asian dust events of April 1998 in East Asia, *J. Geophys. Res.*, *106*(D16), 18346–18359, 2001.
- Prenni, A. J., Petters, M. D., Kreidenweis, S. M., Heald, C. L., Martin, S. T., Artaxo, P., Garland, R. M., Wollny, A. G., and Pöschl, U.: Relative roles of biogenic emissions and Saharan dust as ice nuclei in the Amazon Basin, *Nat. Geosci.*, *2*, 402–405, 2009.
- Prospero, J. M.: Long-term measurements of the transport of African mineral dust to the Southeastern United States: impact on regional air quality, *J. Geophys. Res.*, *104*(D13), 15917–15927, 1999.
- 25 Prospero, J. M., Ginoux, P., Torres, O., Nicholson, S. E., and Gill, T. E.: Environmental characterization of global sources of atmospheric soil dust identified with the NIMBUS 7 total ozone mapping spectrometer (TOMS) absorbing aerosol product, *Rev. Geophys.*, *40*, 1002, doi:10.1029/2000RG000095, 2002.
- 30 Quéré, C. L., Raupach, M. R., Canadell, J. G., Marland, G., Bopp, L., Ciais, P., Conway, T. J., Doney, S. C., Feely, R. A., Foster, P., Friedlingstein, P., Gurney, K., Houghton, R. A., House, J. I., Huntingford, C., Levy, P. E., Lomas, M. R., Majkut, J., Metzl, N., Ometto, J. P., Peters, G. P., Prentice, I. C., Randerson, J. T., Running, S. W., Sarmiento, J. L., Schuster, U., Sitch, S., Takahashi, T., Viovy, N., Van der Werf, G. R., and Woodward, F. I.: Trends in the

4362

- sources and sinks of carbon dioxide, *Nat. Geosci.*, 2, 831–836, 2009.
- Ramanathan, V., Crutzen, P. J., Kiehl, J. T., and Rosenfeld, D.: Aerosols, climate, and the hydrological cycle, *Science*, 294, 2119–2124, 2001.
- Rosenfeld, D., Rudich, Y., and Lahav, R.: Desert dust suppressing precipitation – a possible desertification feedback loop, *P. Natl. Acad. Sci. USA*, 98, 5975–5980, 2001.
- 5 Schepanski, K., Tegen, I., Laurent, B., Heinold, B., and Macke, A.: A new Saharan dust source activation frequency map derived from MSG-SEVIRI IR-channels, *Geophys. Res. Lett.*, 34, L18803, doi:10.1029/2007GL030168, 2007.
- Smirnov, A., Holben, B. N., Eck, T. F., Dubovik, O., and Slutsker, I.: Effect of wind speed on columnar aerosol optical properties at Midway Island, *J. Geophys. Res.*, 108(D24), 4802, doi:10.1029/2003JD003879, 2003.
- 10 Stith, J. L., Ramanathan, V., Cooper, W. A., Roberts, G. C., DeMott, P. J., Carmichael, G., Hatch, C. D., Adhikary, B., Twohy, C. H., and Rogers, D. C.: An overview of aircraft observations from the Pacific Dust Experiment campaign, *J. Geophys. Res.*, 114, D05207, doi:10.1029/2008JD010924, 2009.
- 15 Swap, R., Garstang, M., Greco, S., Talbot, R., and Kallberg, P.: Saharan dust in the Amazon Basin, *Tellus*, 44B, 133–149, 1992.
- Talbot, R. W., Andreae, M. O., Berresheim, H., Artaxo, P., Garstang, M., Harriss, R. C., Beecher, K. M., and Li, S. M.: Aerosol chemistry during the wet season in Central Amazonia: the influence of long range transport, *J. Geophys. Res.*, 95, 16955–16969, 1990.
- 20 Teller, A. and Levin, Z.: The effects of aerosols on precipitation and dimensions of subtropical clouds: a sensitivity study using a numerical cloud model, *Atmos. Chem. Phys.*, 6, 67–80, 2006, <http://www.atmos-chem-phys.net/6/67/2006/>.
- 25 Thomason, L. W., Pitts, M. C., and Winker, D. M.: CALIPSO observations of stratospheric aerosols: a preliminary assessment, *Atmos. Chem. Phys.*, 7, 5283–5290, 2007, <http://www.atmos-chem-phys.net/7/5283/2007/>.
- Todd, M. C., Washington, R., Martins, J. V., Dubovik, O., Lizcano, G., M'Bainayel, S., and Engelstaedter, S.: Mineral dust emission from the Bode'le' Depression, Northern Chad, during BoDEX 2005, *J. Geophys. Res.*, 112, D06207, doi:10.1029/2006JD007170, 2007.
- 30 Twomey, S.: Pollution and the planetary albedo, *Atmos. Environ.*, 8, 1251–1256, 1974.
- Vitousek, P. M. and Sanford Jr., R. L. L.: Nutrient cycling in moist tropical forest, *Annu. Rev. Ecol. Syst.*, 17, 137–167, 1986.

4363

- Washington, R. and Todd, M. C.: Atmospheric controls on mineral dust emission from the Bodélé Depression, Chad, *Geophys. Res. Lett.*, 32(17), L17701, doi:10.1029/2005GL023597, 2005.
- 5 Yu, H. B., Chin, M., Remer, L. A., Kleidman, R. G., Bellouin, N., Bian, H. S., and Diehl, T.: Variability of marine aerosol fine-mode fraction and estimates of anthropogenic aerosol component over cloud-free oceans from the Moderate Resolution Imaging Spectroradiometer (MODIS), *J. Geophys. Res.-Atmos.*, 114, D10206, doi:10.1029/2008JD010648, 2009.

4364

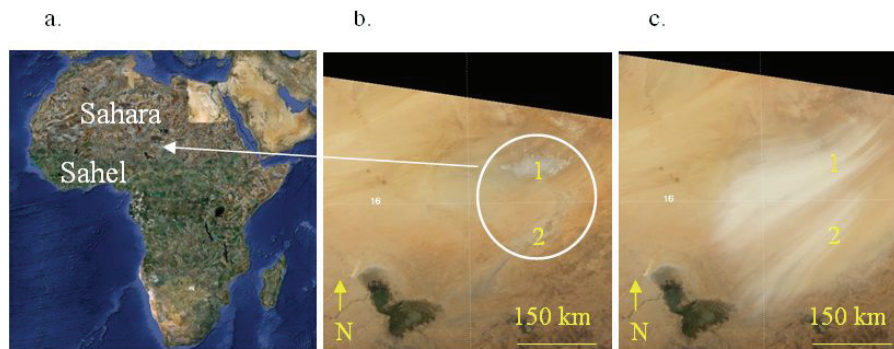


Fig. 1. (a) The location of the Bodélé depression on an image of Africa. (b) The Bodélé depression (composed of two main dust sources, marked in white) on a clear day (5 March 2008) and (c) during dust emission (18 February 2008) as seen by the MODIS instrument on board the Terra satellite.

4365

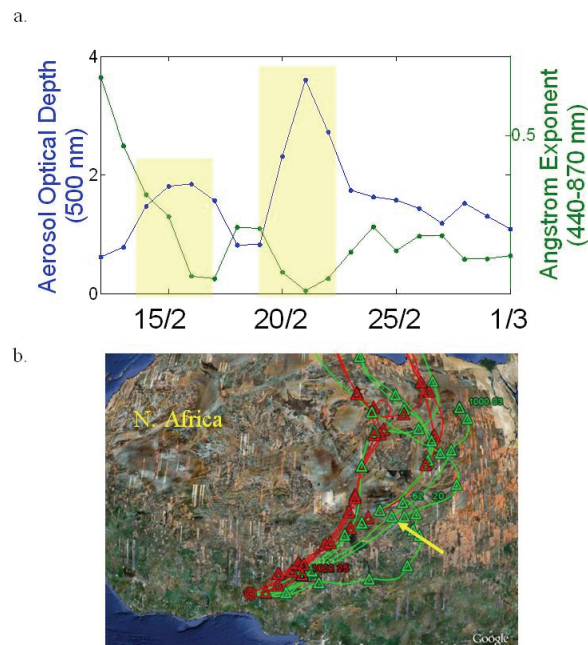


Fig. 2. (a) Level-2 AERONET AOD at 500 nm and Angstrom exponent for 440–870 nm during the period between 12 February and 1 March 2008. Periods of high AOD and low Angstrom exponent are marked with a yellow rectangle; (b) Back trajectories starting from the Ilorin AERONET station (red circle) during 14–16 and 20–22 February, for 850 (green line) and 950 hPa (red line). Triangles mark the location of the air parcel on the previous day. The location of the Bodélé is marked with a yellow arrow. Reanalysis data provided by the NOAA/OAR/ESRL PSD, Boulder, Colorado, USA, from their Web site at <http://www.cdc.noaa.gov/>.

4366

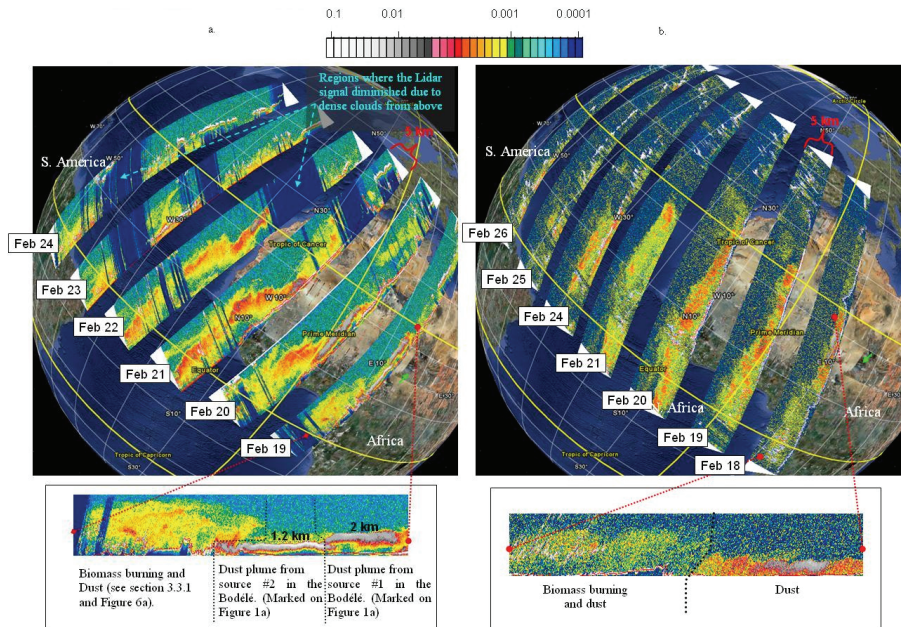


Fig. 3. (a) CALIOP nighttime vertical attenuated backscatter profiles ($\text{km}^{-1} \text{sr}^{-1}$) in the 532 nm band, plotted over the study area. The vertical profiles are 5 km in height (February 2008). The location of the Bodélé is marked by a green arrow. The lower enlargement shows the interaction region between the biomass-burning smoke and the dust plumes. The dust is recognized by the strong backscattering signal relative to the biomass-burning plume (the data was verified with MODIS); **(b)** As Fig. 3a, but for daytime profiles and for 1064 nm wavelength.

4367

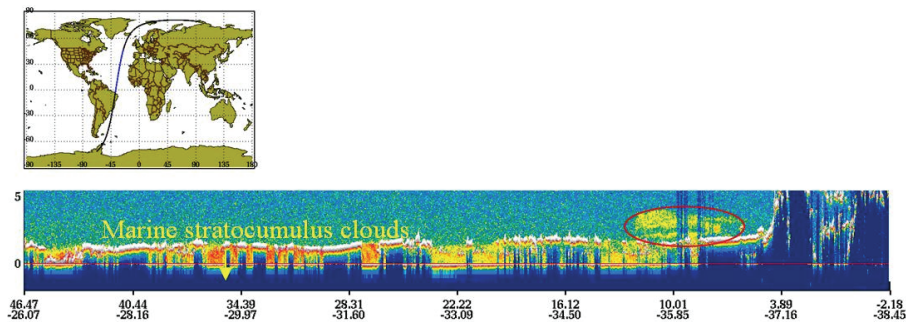


Fig. 4. Vertical profile of CALIOP from 2 February 2008: An example of a CALIOP profile where one can see the height of the marine boundary layer (marked by the height of the marine stratocumulus clouds) with almost no presence of dense aerosol above it. Aerosols above the marine boundary layer are marked by an ellipse. The CALIPSO track is shown on the left.

4368

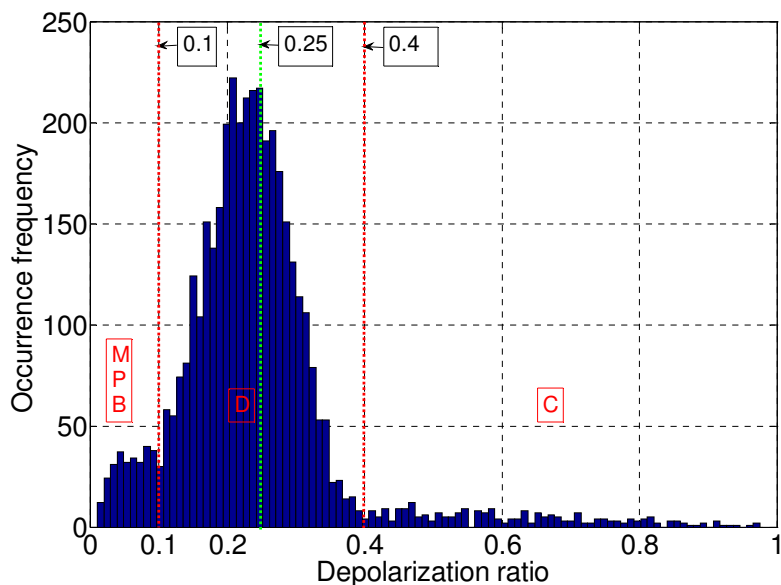


Fig. 5. Frequency of occurrence of depolarization signal, obtained from CALIOP nighttime profiles, from the area covered by the aerosol plumes (as seen in Fig. 3a). The edges of the plumes are defined based on different backscatter patterns (see Sect. 2). Aerosols located in the marine boundary layer (for which the height of the marine boundary layer was defined based on the location of marine stratocumulus clouds, Ben-Ami et al., 2009) were excluded from the analysis, and therefore the depolarization signal obtained from sea salt is expected to be minor. Regions dominated by the depolarization signal from molecules (M), pollution (P), biomass-burning (B), dust (D) and clouds (C) are marked in red. Note that the small peak of depolarization <0.1 was mostly from data taken on 19 February (see Fig. 6b). The threshold for pure dust (0.25) is marked with a green line.

4369

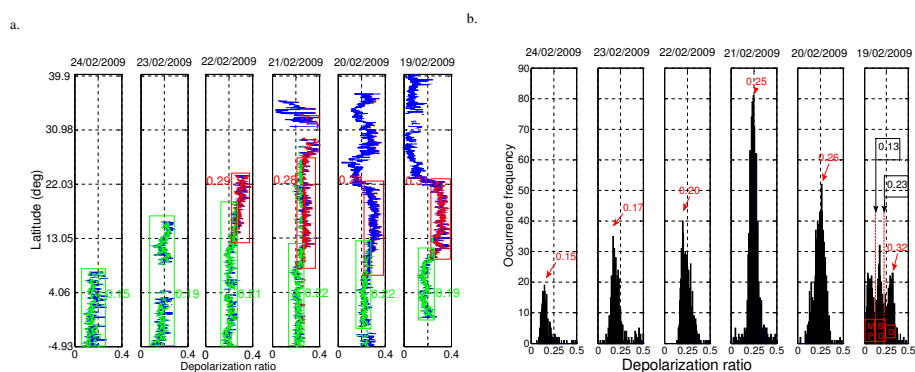


Fig. 6. (a) Averaged depolarization profiles of the aerosol plume. The edges of the plumes are defined based on different backscatter patterns (see Sect. 2). Clouds were removed based on their relatively high depolarization signal and based on their spatial distribution. Aerosols located in the marine boundary layer (the height of the marine boundary layer was defined based on the location of marine stratocumulus clouds, Ben-Ami et al., 2009) were excluded from the analysis. Selected regions of pure dust with depolarization ratio (DR) between 0.25 and 0.4 are marked in red, and regions of biomass aerosol with dust with $0 < DR < 0.25$ are marked in green. Depolarization values (with standard deviation of 0.04) were calculated for the regions designated by the rectangles. **(b)** Frequency of occurrence of depolarization signal (as in Fig. 5, but for all days) obtained from CALIOP nighttime profiles. Rare incidences of depolarization signals >0.5 are not shown.

4370

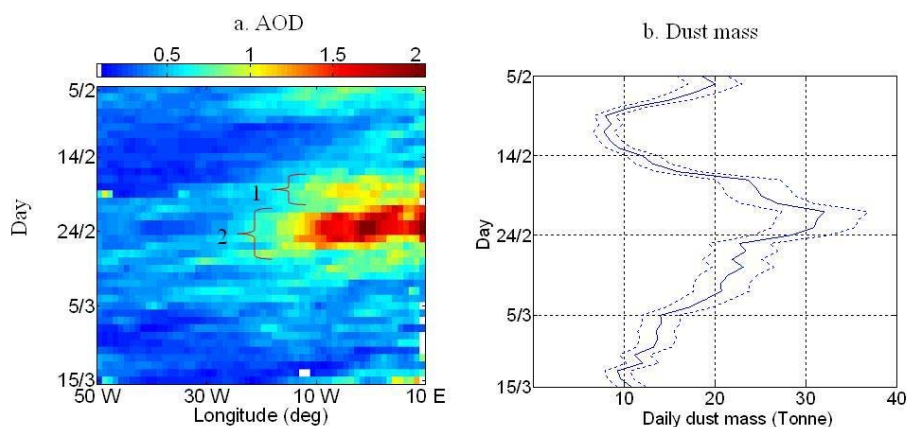


Fig. 7. (a) Daily AOD distribution over the oceanic region. Each line of the figure is a daily latitudinal average (between 10° N–5° S, and 50° W–10° E) that is based on MODIS AOD maps, in spatial resolution of one degree, as obtained from the Aqua and Terra satellites. The signature of dust emitted during (1) 11–16 February and (2) 18–27 February is indicated; (b) Daily estimated dust mass (tonne) over the Atlantic Ocean between 20° N–15° S and 50° W–15° E using Eqs. (1)–(3). Uncertainty in the mass estimates is calculated based on ± 0.4 uncertainty in the 2.7 factor (dashed lines).

4371

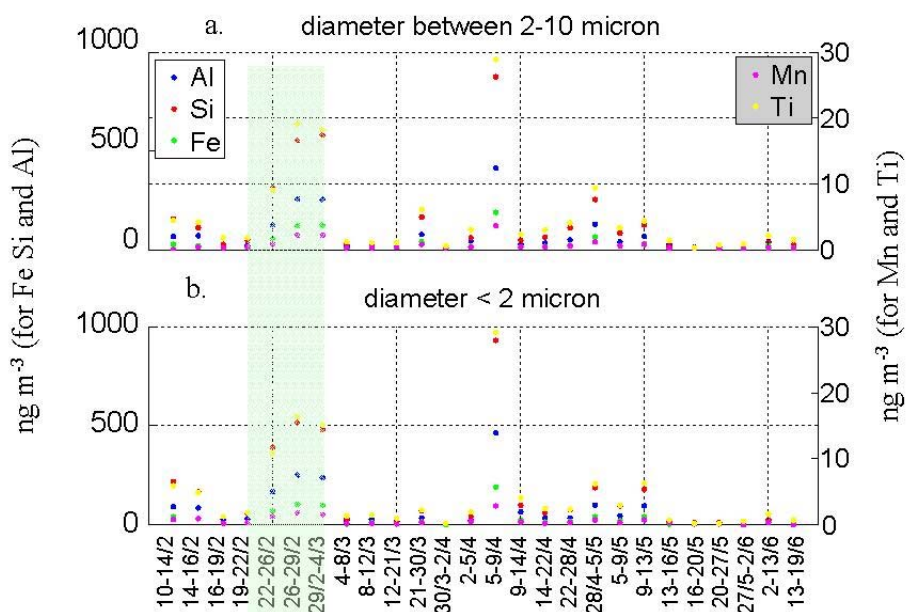


Fig. 8. Elemental composition of aerosol collected at the AMAZE-08 field site in Central Amazonia during February–June 2008, (a) fine (diameter $< 2.0 \mu\text{m}$) and (b) coarse fraction (2.0 to $10 \mu\text{m}$). The areas in the green rectangles mark the dates for which crustal elements were enhanced. The left Y-axis refers to the concentrations of Al, Si, and Fe. The right Y-axis refers to the concentrations of Mn and Ti.

4372